J. Mol. Model. **1996**, *2*, 330 – 340

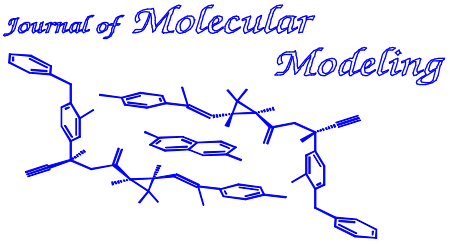

Molecular Dynamics Simulation of a Micellar System

Tim Bast* and Reinhard Hentschke

Max-Planck-Institut für Polymerforschung, Postfach 3148, 55021 Mainz, Germany (bast@mpip-mainz.mpg.de)

Received: 15 May 1996 / Accepted: 6 August 1996 / Published: 27 September 1996

Abstract

We present the results of an atomistic molecular dynamics simulation based on the AMBER/OPLS force field applied to segments of isolated one-dimensional micelles, 2,3,6,7,10,11-Hexa-(1,4,7-Trioxaoctyl)-Triphenylene, in aqueous solution using the SPC/E water model. The quantities which we study include the intra-micellar monomer structure, e.g., the equilibrium monomer-monomer separation along the micelle, the micelle-water interface, which yields the effective micellar diameter, and the flexibility of the micelle in terms of its persistence length as a function of temperature. In addition, we determine the micelle size distribution at low concentration via the free enthalpy gain per monomer-monomer contact using a hydration shell model in combination with thermodynamic integration. Finally, we locate the isotropic-to-nematic transition by using our results as input for an analytical model.

Keywords: MD simulation, micellar system, force field, water models

Introduction

Many amphiphilic molecules in aqueous solution spontaneously self-assemble into labile anisotropic aggregates which exhibit complex liquid-crystalline phase behavior (e.g. [1]). Over the past decade the theoretical modeling of the interplay between self-assembly and lyotropic phase behavior in these systems has been addressed by various authors (e.g. [2] (review article), [3 – 6]). Common to these models is that they focus on rod-shaped micelles (some exceptions are discussed in [2]) and that they are extensions of Onsager's excluded volume theory for the isotropic-to-nematic transition in dilute systems of slender rods. The theoretical models usually depend on a number of a priori unknown parameters such as the monomer shape and size, the flexibility of the micelle expressed in terms of its persistence length (for a rod-like micelle), or the monomer-monomer contact enthalpy within a micelle, etc. These parameters are either adjusted by fitting the model results to the experiment or deduced from independent experimental information. In the present study we want to use the molecular dynamics technique to obtain these parameters via computer simulations.

Today's advanced computer technology allows the modeling of simplified micelles and a fair number of such studies can be found in the literature [7 – 11]. Nevertheless, atomistic molecular modeling on workstation computers is still limited to a few thousand atoms and to the nano-second time scale. This usually prohibits the full simulation of micellar assembly for realistic molecules, and of course the modeling of the phase behavior of such systems. An alternative possibility is to model a small portion of a micelle only using the proper boundary conditions to

* *To whom correspondence should be addressed*

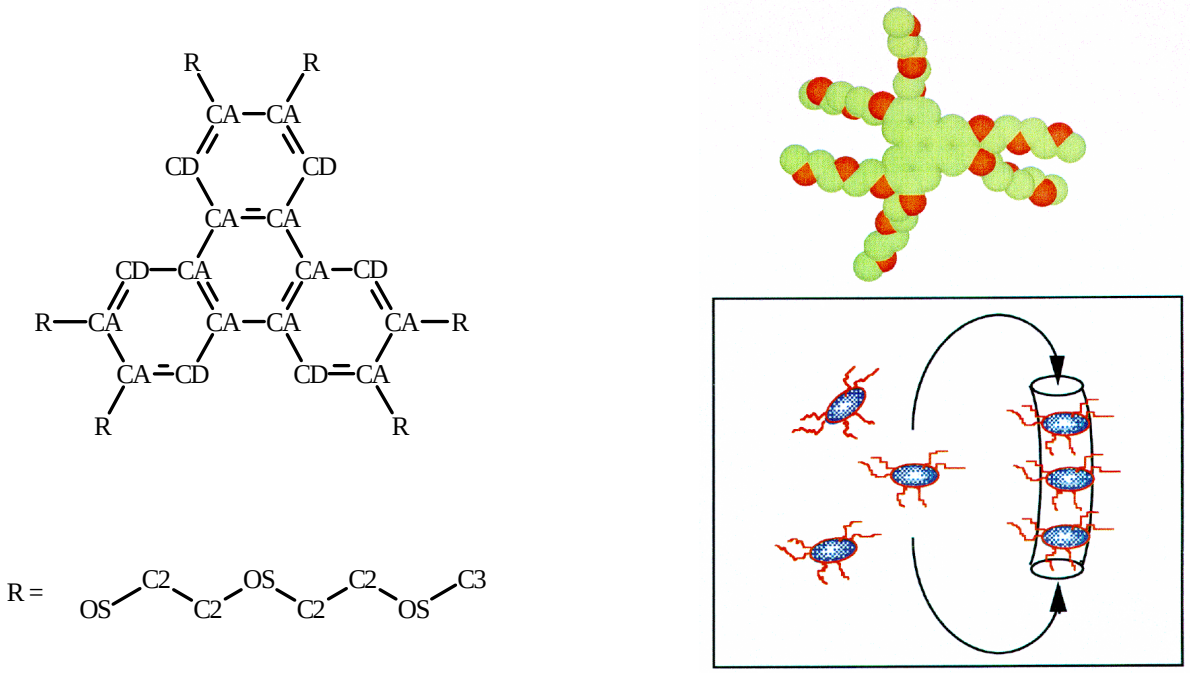

Figure 1. *The 2,3,6,7,10,11-Hexa-(1,4,7-Trioxaoctyl)-Triphenylene (TP6) molecule. Left: The molecular structure is drawn including the atom types corresponding to the notation used in the AMBER force field . Upper right: Van der Waals representation of the TP6 molecule. The green atoms are carbons and the red atoms denote oxygens. Lower right: Sketch of the self-assembly process of TP6 molecules in aqueous solution. The stacking maximizes the contact between the cores of the TP6 molecules.*

extract local information, which then can serve as input to, for instance, analytical theories. This is what we do here. The specific system which we study is 2,3,6,7,10,11-Hexa-(1,4,7-Trioxaoctyl)-Triphenylene (TP6) in water (cf. Figure 1). The monomer is a disk-like molecule consisting of an aromatic core surrounded by hydrophilic side-chains at its periphery. Above the critical micelle concentration the monomers stack, the reason for this is one aspect of this work, and thus reversibly aggregate to form one-dimensional or rod-like micelles (see Figure 1). This system has been studied extensively by Boden and coworkers [12 – 17] (and references therein), which makes it an interesting model system for the above concept for combining theory and simulation.

In the present work we simulate a section of a one-dimensional micelle representing a segment within an isolated, long micelle as well as a complete short micelle both solvated by molecular water. We study the side chain-water interface and deduce the effective diameter of the micelle. In our simulation the length of the simulated micellar segment is allowed to fluctuate freely subject to the external hydrostatic pressure. This allows to determine the equilibrium monomer-monomer separation along the micelle's axis, which is important for relating the aggregation number of a micelle to its length. Using a previously developed approach [18] we use the conformation statistics of the simulated segments to construct long micelles, for which we obtain the persistence length for a number of different temperatures. Furthermore, we study the micelle size distribution via the free enthalpy gain per monomer-monomer contact within a micelle using a thermodynamic integration technique. Finally, we use the results obtained in this study as input parameters for a previously developed analytical model to locate the isotropic-to-nematic transition.

Methodology

In molecular dynamics (MD) simulations the Newtonian equations of motion

$$\frac{d^2}{dt^2}\vec{r}_i = -\frac{1}{m_i}\vec{\nabla}V(\vec{r}_1,\ldots,\vec{r}_N) \quad ; \quad (i = 1\ldots N) \tag{1}$$

are integrated numerically for all N atoms of the system located at positions $\vec{r}_i$ and having masses m_i. Here we employ the program package AMBER 4.0 (Assisted Model Building with Energy Refinement) [19] to compute the corresponding trajectory. The potential V used in AMBER 4.0 consists of five different contributions, i.e.

$$V(\vec{r}_1,\ldots,\vec{r}_N) = \sum_{\text{bonds } i} k_b^{(i)}\left(b_i - b_0^{(i)}\right)^2 + \sum_{\text{angles } i} k_\alpha^{(i)}\left(\alpha_i - \alpha_0^{(i)}\right)^2 + \sum_{\text{dihedrals } i} k_d^{(i)}\left[1 + cos\left(n^{(i)}\phi_i - \gamma^{(i)}\right)\right] + \sum_{\text{atom pairs } ij}\left(\frac{A_{ij}}{r_{ij}^{12}} - \frac{B_{ij}}{r_{ij}^{6}}\right) + \sum_{\text{atom pairs } ij}\frac{q_i q_j}{r_{ij}} \qquad (2)$$

The first two terms model all bond length b_i and valence angle α_i deformations in terms of harmonic potentials. Here we use the SHAKE algorithm to constrain the bond lengths to their equilibrium values $b_0^{(i)}$ [20]. The third term together with the 1-4 non-bonded interactions (cf. below) approximates the torsional potential variations in terms of the torsion angle ϕ_i. The fourth and fifth term describe non-bonded interactions, i.e. Lennard-Jones and Coulomb pair-interactions. The summation over atom pairs includes all atom pairs separated by three (1-4 interactions) or more bonds in the same molecule or atom pairs, where each atom belongs to a different molecule. Note that $r_{ij} = \left|\vec{r}_i - \vec{r}_j\right|$. The non-bonded interactions are only calculated within a residue-based cutoff radius R_{cut}. This means that if two atoms belonging to two different residues are closer than R_{cut}, then all pair-interactions between the two residues are calculated. In the following each water and each TP6 molecule constitute one residue. Note also that in addition the 1-4 interactions are scaled by a factor of ½ [19]. The Lennard-Jones parameters $A_{ij} = \varepsilon_{ij}\sigma_{ij}^{12}$ and $B_{ij} = 2\varepsilon_{ij}\sigma_{ij}^{6}$ for the mixed interactions are obtained via the Lorentz-Berthelot mixing rules $\sigma_{ij} = \sigma_i + \sigma_j$ (where a factor of ½ is absorbed into σ_i and σ_j) and $\varepsilon_{ij} = \sqrt{\varepsilon_i \varepsilon_j}$ [21]. The TP6 molecule is simulated using the united atom representation, whereas the water molecules are described via the SPC/E model [22]. The details of the parameterization and the numerical values of the parameters are given elsewhere [23].

We integrate the equations of motion (1) using the leap-frog verlet algorithm [21] and we apply periodic boundaries using the minimum image convention to calculate the non-bonded interactions. During the simulations temperature and pressure in the simulation box are controlled by the weak coupling velocity scaling thermostat and barostat of Berendsen et al. [24]. However, the pressure is computed for each dimension separately, which is necessary due to the uniaxial anisotropy induced by the presence of the micelle. Then the atom positions are scaled for each dimension separately according to the respective pressures. This anisotropic pressure scaling is necessary because of two different effects. First, water molecules penetrate into the side chains of the micelle and the simulation box thus shrinks. With the pressure scaling perpendicular to the micellar axis we achieve the proper water bulk density away from the micelle (as discussed below in the context of Figure 4). Second, the monomer-monomer separation is a priori unknown. By applying a constant pressure along the micelle any stretch or compression of the micelle is al-

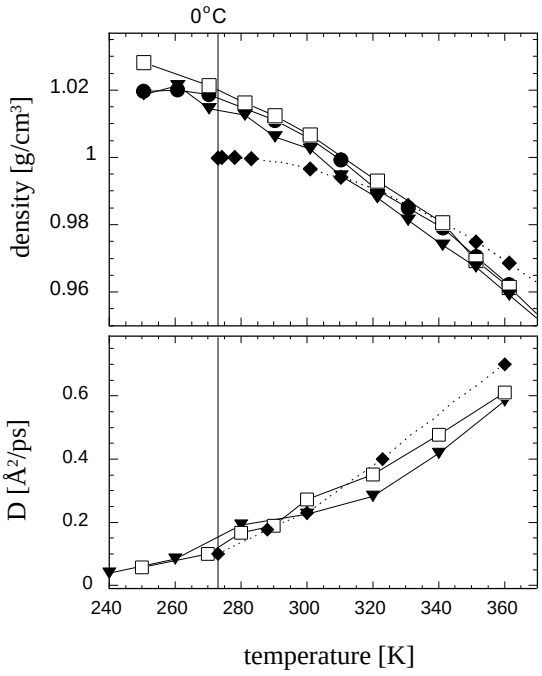

Figure 2. *Test of the SPC/E water model. Upper panel: Simulated water density vs. temperature for different systems, i.e. two different volumes containing 125 (triangles) and 216 (circles and squares) water molecules respectively. For the case of 125 molecules the cutoff radius is R_{cut}=7.5 Å. whereas for the 216 molecules system we compare two different cutoff radii, i.e. R_{cut} = 9 Å (squares) and R_{cut} = 7.5 Å (circles). The experimental values (diamonds) are taken from [25]. Lower panel: Self-diffusion coefficients D of the water molecules vs. temperature for two different box sizes, i.e. 125 molecules using R_{cut} = 7.5 Å (triangles) and 216 molecules using R_{cut} = 9 Å (squares). The experimental values (diamonds) are taken from [26].*

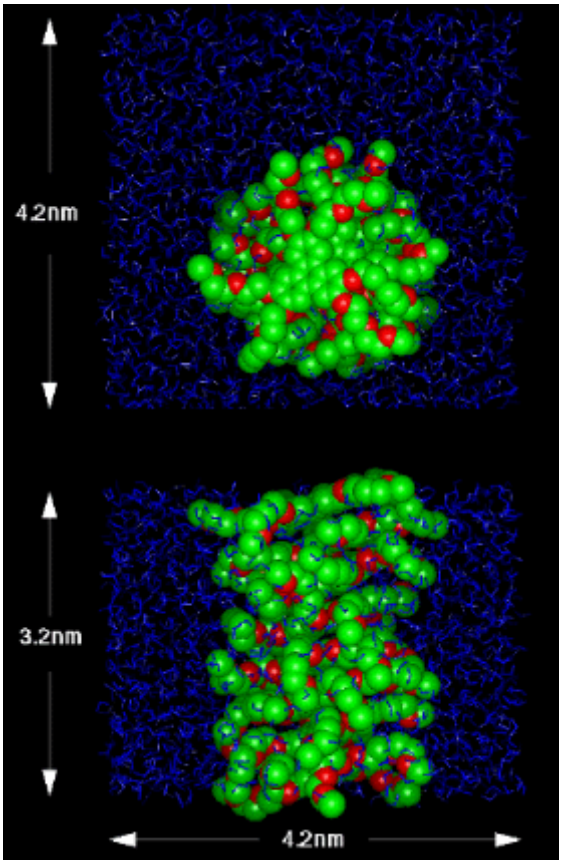

Figure 3. *Snapshot of the simulation box at T = 300 K containing a stack of eight TP6 molecules in van der Waals representation surrounded by water molecules in stick representation. The upper panel shows a view along the micelle's axis, whereas the lower panel shows a side view of the simulation box. Note that due to the application of periodic boundary conditions we model a segment of eight monomers within a virtually infinite micelle.*

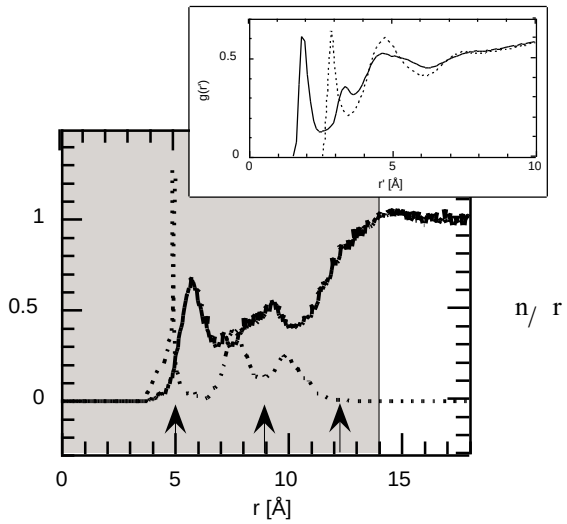

Figure 4. *The radial density distribution of the water oxygen atoms ρ (normalized to its experimental bulk value ρ_0, solid line) and the radial distribution of the side chain oxygen atoms Δn/Δr (in arbitrary units, dotted line) at T = 300 K. Note that r is the radial distance from the micelle's backbone. The arrows indicate the radial positions of the oxygen atoms in a fully extended side chain. From the ρ/ρ_0 curve we estimate a radius of the micelle of 14 Å. The respective area of the plot is shaded. Inset: Side Chain oxygen-water hydrogen pair distribution function g(r') (solid line) and the corresponding side chain oxygen-water oxygen g(r') (dotted line).*

lowed to relax, and the average monomer-monomer separation can fluctuate around its equilibrium value.

Test of the water model

Figure 2 summarizes the results of several 0.5ns constant pressure test simulations of pure SPC/E water [22] for different box sizes (i.e., 125 and 216 water molecules) at various temperatures ranging from 250K to 360K. Figure 2(a) shows the simulated density as a function of temperature in comparison to the experiment [25]. The deviation of the liquid densities from their experimental values is always less than 2%. For 216 water molecules and at $T > 300$K the deviation is even less than 1%. Also, for 216 water molecules the figure includes the results for two different values of the cutoff radius, i.e. $R_{cut} = 7.5$ Å and $R_{cut} = 9$ Å. The reduction of the cutoff radius leads to a very minor decrease in density due to the neglect of attractive interactions. Figure 2(b) shows the corresponding temperature dependence of the self-diffusion coefficient, *D*, in comparison to the experiment [26]. For liquid water the self-diffusion coefficients are in very good agreement with the experimental data, especially in the temperature range which is of interest in this work (T=280…300K). Notice, that we do not observe any indication of freezing in the simulated temperature range below 273K. The O-O pair correlation function, which is not shown here, is very similar to that obtained in Monte Carlo studies [27]. The positions of the first three peeks of the experimental curve are reproduced to within 0.1 Å. Only the height of the first peak is somewhat exaggerated (roughly by 30 %).

The TP6/water system

For the various simulations in this work which include TP6 the starting configurations are prepared as follows. Stacks consisting of six and eight TP6 molecules are assembled by first building and energy-minimizing a single TP6 mol-

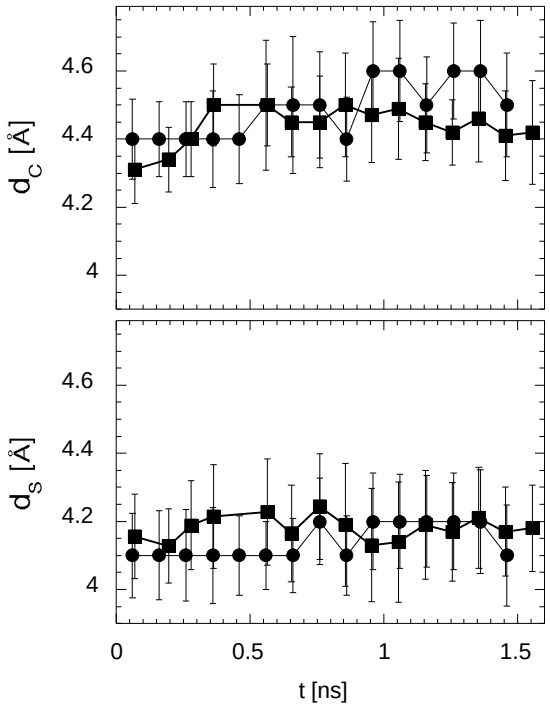

Figure 5. *Upper panel: Center of mass separation d_C between adjacent monomers in the 8-micelle vs. simulation time t. Lower panel: Corresponding stacking distance d_S vs. simulation time t. The stacking distance is the center of mass separation projected onto the backbone of the micelle. Circles: T = 280 K; squares: T = 300 K. All values are obtained by averaging over all monomer-monomer contact sites within the micelle as well as over 100 ps timeslices along the trajectory. The error bars denote the standard error assuming that the contact sites are independent of each other.*

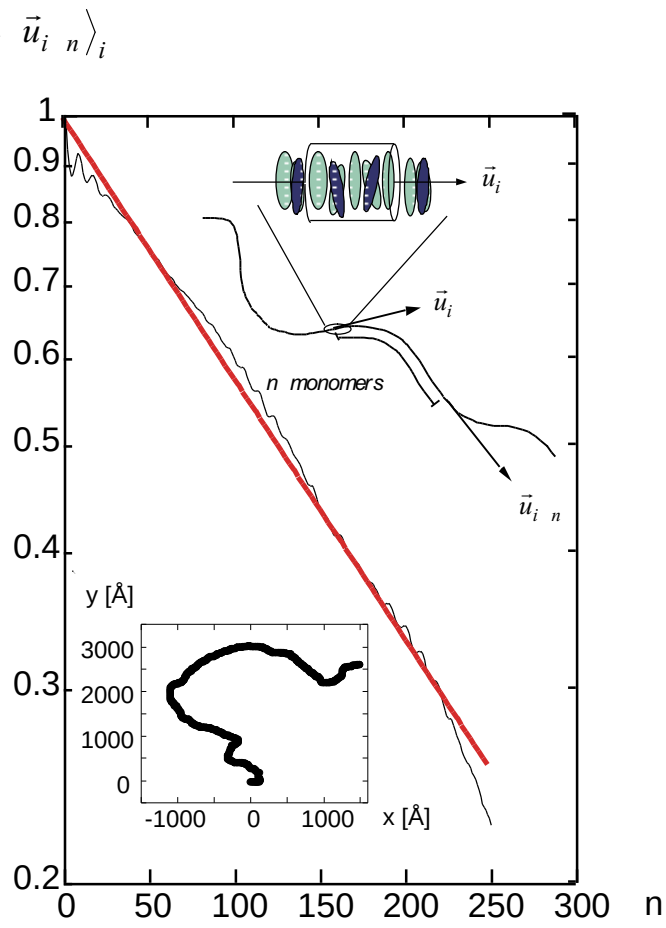

Figure 6. *Orientation correlation function $\langle \vec{u}_n \cdot \vec{u}_{i+n} \rangle_i$ vs. distance n. The $\vec{u}_i$ and $\vec{u}_{i+n}$ are tangent vectors along the micelle's contour at monomers i and i+n. The average is taken over i. The smooth straight line is an exponential fit to the simulation result for T = 300 K. Upper right insert: Definition of a tangent vector along the micelle's contour. Lower left insert: x,y-Projection of the contour of one large micelle.*

ecule with the program INSIGHT II using the Discover version 3.2 force field [28]. The TP6 molecule is then replicated employing a 4 Å repeat distance perpendicular to the triphenylene plane. Subsequently, the stacks are surrounded by water molecules placed on a simple cubic lattice. The box with the 6-mer contains 2500 water molecules whereas the box with the 8-mer contains 1827 water molecules. Note that both systems are prepared large enough to include bulk behavior of the water at large radial separations from the micelle. In the case of the 6-micelle this is also true along the axial direction. Notice also that we apply a constant pressure of 1bar to the box. In the case of the 8-micelle the axial box dimension coincides with eight times the monomer-monomer separation. The latter, however, is flexible due to the constant pressure condition. Note that because of periodic boundary conditions the 8-mer corresponds to a segment of a virtually infinite micelle. In a similar fashion a third system is prepared which contains two isolated TP6 molecules solvated in 2004 water molecules.

The results reported below are for MD simulations at three different temperatures (T = 280, 290 and 300 K). After a short 10 ps MD run using a 1fs time step the remainder of each simulation is carried out with a 4fs time step. The total length of each run is between 0.6 and 1.5ns during which the atom positions are stored every 0.2 ps. As an example, Figure 3 shows an instantaneous configuration during the simulation of the 8-mer. The eight monomers in

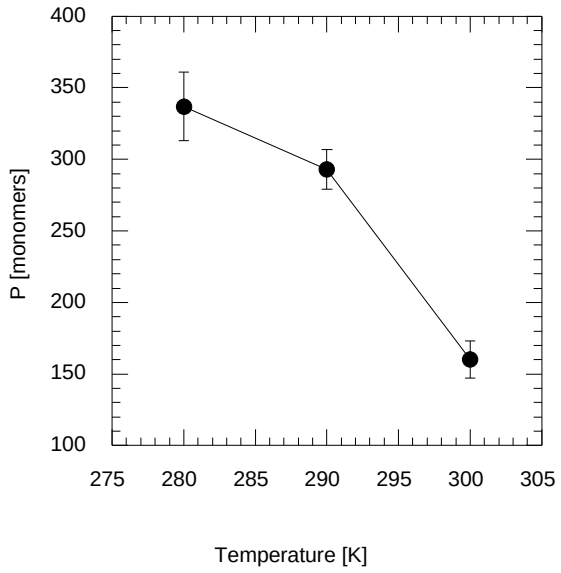

Figure 7. *Average persistence length, P, for the constructed long micelles vs. temperature T for three different temperatures.*

the box form a stack with the core regions in contact. Notice that the water molecules penetrate into the side chains but do not enter the core region.

The side chain-water interface

In Figure 4 the radial density distributions of the water oxygen atoms and the radial distribution of the side chain oxygen atoms are shown. Note that the water oxygen density is normalized to its experimental bulk value. The results plotted in Figure 4 are taken from the trajectory at T = 300 K. The radial distributions extracted from the other two trajectories do not show significant deviations from the curves shown in Figure 4. The radial distribution function of the water molecules shows two peaks at a distance of r = 6 Å and r = 9.5 Å. In this range the average density is approximately half that of the bulk value, which is approached in the range 11 Å < r < 14 Å. From this we estimate a micelle diameter of about 28 Å. Notice that an appreciable onset of the water distribution occurs at r = 4 Å, i.e. these water molecules are right at the periphery of the triphenylene core. However, the water molecules do not penetrate into the core region between the monomers.

The corresponding radial distribution of the side chain oxygen atoms shows three peaks which can be identified with the three oxygen atoms in each side chain. The first peak is sharp, whereas the broadness and the inward shift of the two outer peaks reflects the conformational freedom of the side chains. Notice that the arrows in Figure 4 denote the radial oxygen positions in a fully extended side chain.

Table 1. *Mean values for the center of mass separation d_C and the stacking distance d_S between two adjacent monomers for the three different temperatures.*

T [K]	$\langle d_C \rangle$ [Å]	$\langle d_S \rangle$ [Å]
280	4.5 ± 0.14	4.2 ± 0.12
290	4.5 ± 0.19	4.3 ± 0.20
300	4.4 ± 0.10	4.2 ± 0.13

Comparing the two radial distributions it can be seen that the radial density of the water oxygens shows local minima at the preferred positions of the side chain oxygen distribution peaks. The oxygen atoms in the water molecule as well as in the side chains carry negative partial charges. Therefore, a repulsive Coulomb force acts between these atoms. This force explains the minima mentioned above. Nevertheless, there appear to exist hydrogen bonds between the neighboring water molecules and the side chain oxygen atoms. This can be seen from the pronounced first peak at ≈ 1.9 Å in the side chain oxygen – water hydrogen pair distribution function shown in the inset of Figure 4.

Monomer-monomer stacking distance

The monomer-monomer distance in the micellar aggregates is important in converting aggregation numbers into the actual lengths of the micelles. These lengths play an important role in the analytical description of the phase behavior of TP6 in aqueous solution. Here we study two differently defined monomer-monomer separations. In the first case we determine the separation of the centers of mass d_C of adjacent triphenylene cores. In the second case we compute the projection of the previously determined separation d_C onto the backbone in order to obtain the stacking distance d_S along the backbone. In this study we define the backbone of the micelle as the principal axis of inertia corresponding to the direction along the micelle.

Figure 5 shows d_C and d_S averaged over the monomer-monomer contacts within the periodic 8-micelle as a function of simulation time t for two temperatures, i.e. T = 280 K and T = 300 K, which bracket the temperature range investigated here. The average over all contacts for the separations d_C and d_S are given in Table 1. On average d_C exceeds d_S by 0.2 to 0.3 Å. However, we do not see any change of the mean distances with temperature exceeding the error margin. Thus, the magnitude of the error, where we assume that different contacts are statistically independent, is certainly an upper limit for the temperature dependence of d_C and d_S. It is worth noting that the averages for d_C and d_S in Table 1 are rather close to the experimentally determined ring-ring separation of between ≈ 4.2 Å at T = 280 K and 5 Å at T = 300 K [17].

Note that we compare the results obtained for the infinite micelle with those for the micelle consisting of six monomers only. Within the fluctuations we do not observe any difference neither in d_C nor in d_S between the short and the infinite micelle.

Micellar flexibility

To obtain the flexibility of the rod-like micelle we estimate its persistence length, *P*. *P* is defined by the correlation between the tangent vectors along the micelle (see upper inset of Figure 6). For not too small separations the correlation for two tangent vectors $\vec{u}_i$ and $\vec{u}_{i+n}$ separated by *n* monomers is given by [29]

$$\langle \vec{u}_i \cdot \vec{u}_{i+n} \rangle_i = e^{-n/P} \tag{3}$$

In order to compute the persistence length via this equation a large micelle is required to compute the average in (3). Here we use an adaptation of a method, which we have developed previously to compute *P* for a helical polypeptide (Poly-γ-benzyl-L-glutamate) [18]. The method is a build-up procedure by which a long micelle is constructed by chaining together instantaneous conformations taken from a simulation of a short segment, i.e. the 8-micelle in the present case.

The persistence length is then calculated using equation (3) by averaging the dot products of the tangent vectors $\vec{u}_i$ and $\vec{u}_{i+n}$ along the micelle. The direction of each tangent vector is defined as the moment of inertia axis along a cylindrical segment of the micelle consisting of five monomers centered at the origin of the tangent vector (cf. inset in the upper right of Figure 6). As a measure of the uncertainty of the persistence length to be computed we calculate the standard deviation of *P* based on ten different long micelles each constructed as described by choosing at random ten different initial segments. Figure 6 shows an exponential fit to $\langle \vec{u}_n \cdot \vec{u}_{i+n} \rangle_i$ for one of the ten micelles at T = 300 K. The lower left inset of Figure 6 shows an example micelle in terms of its contour's *x*,*y*-projection.

In Figure 7 the mean value of the persistence length is shown for three different temperatures. It can be seen that the persistence length decreases with increasing temperature. Thus, the micelles become more flexible with rising temperature. The error bars denote the standard error as explained above.

Thermodynamics of micellar assembly

To good approximation the chemical potential μ_n of a one-dimensional n-micelle in dilute solution can be written as

$$\mu_n = n\tilde{\mu}_n^0 + RT\ln\left(\tfrac{1}{n}X_n\right) + RT\ln\gamma - \alpha RT(n-1) \tag{4}$$

An extensive discussion of this equation can be found in the article by A. Ben-Shaul and W.M. Gelbart in reference [1]. In the first term $\tilde{\mu}_n^0$ is a standard average chemical potential per monomer in an n-micelle, excluding the interaction between the monomers, which is treated separately. The second term is the contribution due to the solute mixing entropy. Note that here X_n refers to the mole fraction of monomers within micelles of aggregation number n. In particular n = 1 corresponds to the free monomers. The third term describes the interaction between the solute particles. However, here we are merely interested in the limit of no interaction, where the activity coefficient g = 1 so that this term vanishes (At high concentrations, however, excluded volume effects as well as entropic repulsion between the persistent-flexible micelles due to their confinement must be included). The last term constitutes a simple one-parameter model of monomer-monomer interaction within a one-dimensional *n*-micelle, where *n*-1 is the number of contacts between monomers. The quantity –a is the molar free enthalpy per monomer-monomer contact and RT, i.e.

$$\alpha = -\frac{\Delta G_{contact}}{RT} \tag{5}$$

which in general depends on the type of solvent, temperature, pressure etc. and usually also on *n*, because monomers near the end of a micelle feel a different environment compared to those in the bulk of the micelle. Here, however, we will be exclusively dealing with the bulk value of α, which is independent of *n*. Using equation (4) in conjunction with the equilibrium condition $\mu_n = n\mu_1$ yields the micellar size distribution

$$X_n = nX_1^n e^{\alpha(n-1)+n\left(\tilde{\mu}_1^0 - \tilde{\mu}_n^0\right)/RT} \tag{6}$$

under the given conditions. In the following we will be concerned with the calculation of α or rather $\Delta G_{contact}$, which, as equation (6) shows, is an important ingredient for the calculation of the micellar size distribution. Also, the analysis of the experimental data in reference [17] indicates that for the present system the approximation $\tilde{\mu}_1^0 = \tilde{\mu}_n^0$ seems to be justified, and that the size distribution is mainly determined by α alone.

In the following we apply the simulated thermodynamic integration approach (cf. e.g. [30]), which allows to evaluate $\Delta G_{contact}$ via the relation

$$\Delta G_{contact} = \frac{1}{n-1}\int_{\infty}^{\lambda_{eq}} \left\langle \frac{\partial H_c}{\partial \lambda} \right\rangle_{\lambda} d\lambda \tag{7}$$

Here $H_C(\lambda)$ is the Hamiltonian of the system with a fixed monomer-monomer separation λ. $\langle \ldots \rangle_{\lambda}$ denotes an ensemble average at the same fixed λ. The numerical integration of the right hand sight of equation (7) requires a series of MD simulations to evaluate the ensemble average at several distinct values of λ. However, the method is computationally too expensive for the complete system containing the micelle and the solvent. Therefore we calculate $\Delta G_{contact}$ along the alternative route (double lined arrows) in the following thermodynamic cycle

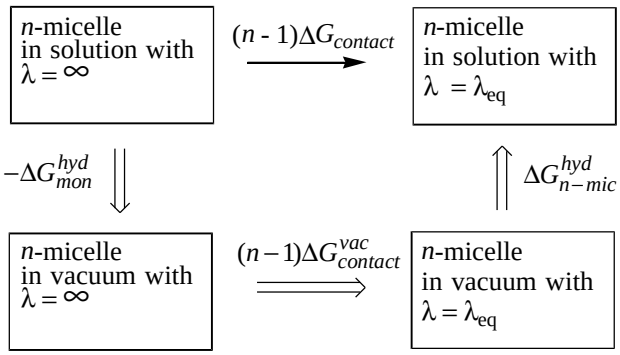

(8)

i.e.

$$(n-1)\Delta G_{contact} = -n\Delta G^{hyd}_{mon} + (n-1)\Delta G^{vac}_{contact} + \Delta G^{hyd}_{n-mic} \tag{9}$$

Here ΔG^{hyd}_{mon} and ΔG^{hyd}_{n-mic} are the free enthalpies of hydration of the monomer and the n-micelle, respectively, whereas $\Delta G^{vac}_{contact}$ is $\Delta G_{contact}$ in vacuum. Note that $\Delta G^{vac}_{contact}$ requires substantially less computational effort, because without solvent the number of interactions is greatly reduced.

To obtain the hydration free enthalpies of the micelle ΔG^{hyd}_{n-mic} from our trajectories we use the hydration shell model developed by Scheraga and co-workers [31, 32]. It is based on the assumption that ΔG^{hyd} can be split up in contributions proportional to the average water accessible volume $< V_{(i)k} >$ of the individual atoms or groups. Making the simplifying assumption that the weighting of the sidechain conformations in solution is the same as in vacuum it can be written

$$\Delta G^{hyd} \approx \sum_k \Delta g^{hyd}_k \left\langle V_{(i)k} \right\rangle \tag{10}$$

Δg^{hyd}_k is the hydration free enthalpy density of the kth atom or group. Note that these densities are independent of the molecule's conformation. The $< V_{(i)k} >$ can be obtained directly from our simulation trajectory by Monte Carlo integration. The hydration free enthalpies of the monomer ΔG^{hyd}_{mon} are obtained in a similar fashion except that the trajectories are taken from three additional simulations of two isolated TP6 molecules in water.

Note that the righthand side of equation (7) is the reversible work necessary to separate a monomer from the micelle. Here we evaluate the righthand side of (7) in vacuum by calculating

$$\Delta G^{vac}_{contact} = \int_{\infty}^{\lambda_{eq}} \left\langle f^{vac}_{ax} \right\rangle_{\lambda} d\lambda \tag{11}$$

where $\left\langle f^{vac}_{ax} \right\rangle_{\lambda}$ is the time averaged force along the axis of the micelle in vacuum acting on a monomer, which is pulled off the end of the micelle. The micelle is approximated by a trimer for which we perform molecular dynamics simulations (as discussed above) constraining the positions of the carbon atoms of the central hexagon in each monomer so that these hexagons in neighboring monomers

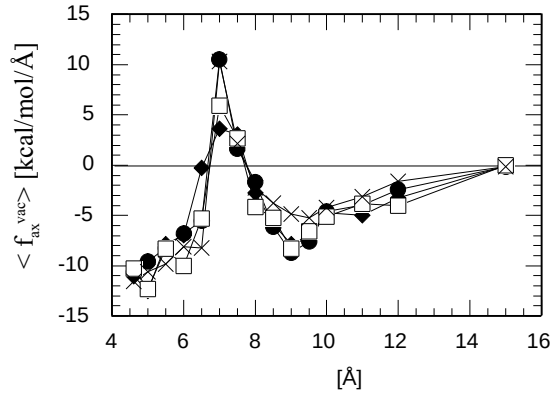

Figure 8. *Time averaged contact force* $\left\langle f^{vac}_{ax} \right\rangle_{\lambda}$ *as a function of* λ *for three different temperatures T = 280 K (squares), 290 K (diamonds), and 300 K (circles). For comparison, the result of a similar calculation for T = 300 K only with a different charge model (AM1 charges) is also shown (crosses). All points are averages over MD trajectories of 0.5 ns.*

Table 2. *Free enthalpies calculated along the alternate path in (9), and* $\Delta G_{contact}$ *and* α *calculated according to (9) and (5) respectively in the limit for large n.*

ΔG [kcal/mol]	**T = 280 K**	**T = 290 K**	**T = 300 K**
ΔG^{hyd}_{mon}	-47.8	-47.6	-48.4
$\frac{1}{n}\Delta G^{hyd}_{n-mic}$	-29.3	-29.4	-29.8
$\Delta G^{vac}_{contact}$	-43	-38	-35
$\Delta G_{contact}$	-24.5	-19.8	-16.4
α	43.9	34.3	27.4

are eclipsed and parallel. All other atoms of the triphenylene core and in particular the side chains remain unconstrained. Initially, we set the distance of the triphenylene to the equilibrium separations discussed above. Subsequently, the monomer is pulled away along the axis of the micelle, and $\left\langle f^{vac}_{ax} \right\rangle_{\lambda}$ is calculated as a function of λ.

Table 2 lists the hydration contribution to $\Delta G_{contact}$ according to equation (10). Thus in the indicated temperature range the hydration contribution to $\Delta G_{contact}$, $-\Delta G^{hyd}_{mon} + \frac{1}{n}\Delta G^{hyd}_{n-mic}$, is close to 18.5kcal/mol which means that the hydration disfavors micelle formation. Table 2 also contains the values of $\Delta G^{vac}_{contact}$ calculated according to (11) – the corresponding $\left\langle f^{vac}_{ax} \right\rangle_{\lambda}$ vs. λ curves are shown in Figure 8. The values for $\Delta G^{vac}_{contact}$ obtained in this fashion range from –43 kcal/mol for T = 280 K to –35 kcal/mol for T = 300 K. Note that the decrease in $\Delta G^{vac}_{contact}$ with decreasing temperature is physically reasonable, because the entropic repulsion (due to spatial confinement) between the sidechains should become less as temperature decreases. The resulting values for $\Delta G_{contact}$ yield an α (cf. Table 2) which is between 43.9 for T = 280 K and 27.4 for T = 300 K, and thus our α is about two to three times larger than the experimental value quoted above.

One source of error in the present calculation is the neglect of the polarization contribution to ΔG^{hyd} in equation (10). The parameterization is strongly model dependent and unfortunately cannot be carried over to the model used in this work. We also probe the sensitivity of $\left\langle f^{vac}_{ax} \right\rangle_{\lambda}$ to the charge model, because the partial charges are a possible source of considerable error in every force field calculation. Figure 8 shows the integrand on the righthand side of (11) for T = 280, 290, 300 K. All three curves show a similar behavior with a positive (repulsive) maximum at $\lambda \approx 7$ Å. We test the sensitivity of $\left\langle f^{vac}_{ax} \right\rangle_{\lambda}$ on the partial charges by comparing the result for the partial charges of the Q-equilibration algorithm, which we use here, to the result for AM1 charges (which on average are 2.6 × smaller). Overall we find little difference in the $\left\langle f^{vac}_{ax} \right\rangle_{\lambda}$ *vs.* λ curves, and thus the corresponding areas under the curves are close, and we would estimate the error at about 10%. Thus, if the error for ΔG^{hyd}_{mon}, $\frac{1}{n}\Delta G^{hyd}_{n-mic}$ and $\Delta G^{vac}_{contact}$ in Table 2 is 10%, then the resulting error for α is already about 25%, becaused $\Delta G^{vac}_{contact}$ essentially is calculated as the difference between significantly larger numbers.

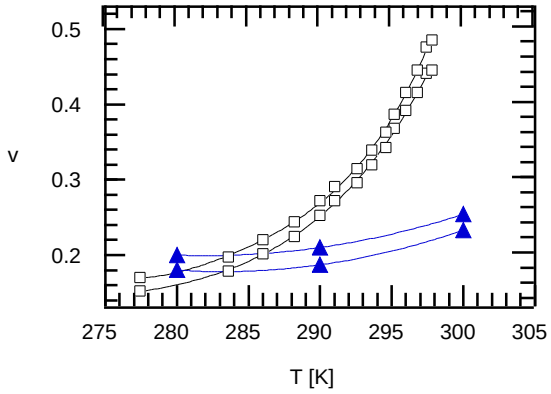

Figure 9. *The isotropic-to-nematic phase coexistence region in terms of temperature T and solute volume fraction* υ *obtained in this study (triangles) and experimentally (squares).*

Isotropic-to-nematic phase transition

In [33] a theoretical model for the phase behavior including the isotropic-to-nematic phase transition for a system of reversibly assembling long, rod-like, flexible, monodisperse, linear aggregates is given. The phase behavior is driven by a subtle interplay between aggregate flexibility, the inter-aggregate steric interactions, and the internal energy of the aggregates. The orientation free energy in the model depends on the angular distribution of the aggregate's contours and on their length. The flexibility of the aggregates therein is characterized by their

persistence length. For the contribution due to the excluded volume an extension of Parson's decoupling approximation (cf. [34]) is used. This expression simplifies to Onsager's trial function description [35] of long, rigid rods for small volume fractions of the solute. Finally, the internal free energy of the aggregate is described via a monomer-monomer contact free energy analogous to the last term in equation (4).

Figure 9 shows a preliminary calculation, where we have converted the theoretical isotropic-nematic phase diagram of Figure 3 in reference [33] from the P-υ-plane to the T-υ-plane, using the simulation result of Figure 7. Here υ is the solute (TP6) volume fraction. The comparison with the experimental transition [16] is rather satisfactory at the low temperatures, but for higher temperatures the deviation is considerable. We mainly attribute this to the independence of α on temperature and concentration assumed in [33], and, in addition, to the neglect of polydispersity in the analytical model.

Conclusion

In this paper we have studied the structure and thermodynamics of a rod-like micelle using molecular dynamics simulations. From the radial water density profile and the radial positions of the side chain atoms we estimate the effective diameter of the TP6 micelle in water to be 28 Å. For the average monomer-monomer center of mass and stacking distance within the micelle we obtain 4.5 Å and 4.2 Å respectively for all three temperatures considered here. These average values are in good agreement with the experimentally determined ring-ring separations. Long TP6 micelles are flexible, and we obtain persistence lengths between ≈ 340 monomers at 280 K and ≈ 160 monomers at 300 K. It is worth mentioning that the temperature dependence of the phase behavior of micellar systems like the one studied here enters mainly through two quantities - the persistence length and the contact free enthalpy. Here we have shown that the temperature dependence of the first is rather strong in the case of TP6 in water, i.e. P is reduced by a factor of ≈ 2 between T = 280 K and 300 K. Thus, the decrease of the persistence length with increasing temperature is substantial. As mentioned before, the effective micelle diameter as well as the persistence length are key quantities in the theoretical description of the phase behavior of the TP6/H_2O-system, i.e. excluded volume interactions are dependent on the micelle's geometry (aspect ratio), whereas the orientation distribution of the micelle's contour and the attendant entropy contribution depend on the persistence length and on the micelle's contour length which in turn depends on the monomer-monomer separation. The present simulation shows how, even for a large system (in terms of the monomer size), these quantities can be calculated including microscopic detail. Furthermore, we have considered the monomer-monomer contact free enthalpy which largely governs the micellar size distribution at low concentration. We base this calculation on a combination of our simulation trajectories with a hydration shell model due to Scheraga and co-workers. Even though our simulation results of α = 27.4 43.9 overestimate the experimental findings they allow to compare the various contributions to the monomer-monomer contact free enthalpy. We find that the main contribution to α is due to the competition between the monomer contact potential energy (which favors micellation) and the loss of free enthalpy of hydration when a monomer-monomer contact is formed (which disfavors micellation). Finally, we used our simulation results as an input for an previously developed theoretical model for the phase behavior of reversibly assembling, rod-like, flexible aggregates. In this preliminary calculation we have found quantitative agreement for T = 280 K and qualitative agreement for the two higher temperatures.

References

1. Micelles, Membranes, Microemulsions and Monolayers, Gelbart, W. M.; Ben-Shaul, A. and Roux, D. (eds.) Springer, New York, **1994**.
2. Taylor, M. P. and Herzfeld, J. *J. Phys.: Condens. Matter* **1993**, *5*, 2651.
3. McMullen, W. E.; Gelbart, W. M. and Ben-Shaul, A. *J. Chem. Phys.* **1985**, *82*, 5616.
4. Odijk, T. *J. Physique* **1987**, *48*, 125.
5. Hentschke, R. *Liq. Cryst.* **1991**, *10*, 691.
6. van der Schoot, P. and Cates, M. E. *Europhys. Lett.* **1994**, *25*, 515.
7. Böcker, J.; Brickmann, J. and Bopp, P. *J. Phys. Chem.* **1994**, *98*, 712.
8. Rector, D. R.; van Swol, F. and Henderson, J. R. *Mol. Phys.* **1994**, *82*, 1009.
9. Laaksonen, L. and Rosenholm, J. B. *Chem. Phys. Lett.* **1993**, *215*, 429.
10. Shelley, J. C.; Sprik, M. and Klein, M. L. *Langmuir* **1992**, *9*, 916.
11. Karaborni, S.; Esselink, K.; Hilbers, P. A. J.; Smit, B.; Karthäuser, J.; van Os, N. M. and Zana, R. *Science* **1994**, *266*, 254.
12. Boden, N.; Bushby, R. J. and Hardy, C. *J.Phys. Lett. Paris* **1985**, *46*, L 325.
13. Boden, N.; Bushby, R. J.; Hardy, C. and Sixl, F. *Chem. Phys. Lett*. **1986**, *123*, 359.
14. Boden, N.; Bushby, R. J.; Jolly, K. W.; Holmes, M. and Sixl, F. *Mol. Cryst. Liq. Cryst*. **1987**, *152*, 37.
15. Ferris, L. M. *Ph.D. thesis*, University of Leeds, **1989**.
16. Edwards, P. J. B. *Ph.D. thesis*, University of Leeds, **1993**.
17. Hubbard, J. and Boden, N. privat communication.
18. Helfrich, J.; Hentschke, R. and Apel, U. M. *Macromolecules* **1994**, *27*, 472.

19. Pearlman, D. A.; Case, D. A.; Caldwell, J. C.; Seibel, G. L.; Singh, U. C.;Weiner, P. K. and Kollman, P. A. AMBER 4.0, Molecular Dynamics Simulation Package, University of California, San Francisco, **1991**.
20. Ryckaert, J. P.; Cicotti, G. and Berendsen, H. J. C. *J. comput. Phys*. **1977**, *23*, 327.
21. Allen, M. P. and Tildesley, D. J. *Computer Simulations of Liquids*. Oxford University Press, Oxford, **1987**.
22. Berendsen, H. J. C.; Grigera, J. R. and Straatsma, T. P. *J. Phys. Chem*. **1987**, *91*, 6269.
23. Bast, T. and Hentschke, R. *J. Phys. Chem*. **1996**, in print.
24. Berendsen, H. J. C.; Postma, J. P. M.; van Gunsteren, W. F.; DiNola, A. and Haak, J. R. *J. Chem. Phys*. **1984**, *81*, 3684.
25. Riddick, J. A.; Bunger, W. B. and Sakano, T. K. *Organic Solvents*, John Wiley & Sons, New York, **1986**.
26. Landolt-Börnstein, Vol. 5: Eigenschaften der Materie in ihren Aggregatzuständen, Schäfer, K. (ed.), Springer, Berlin, Heidelberg, New York, **1969**.
27. Jorgensen, W.; Chandrasekhar, J.; Madura, J.; Impey, R. and Klein, M. *J. Chem. Phys*. **1983**, *79*, 926.
28. INSIGHT, Vers. 2.0, Molecular Dynamics Simulation Software, Biosym Technologies, **1989**.
29. Landau, L. D. and Lifshitz, E. M. *Statistische Physik*, Teil 1, Akademie Verlag, Berlin, **1979**, Vol. 5.
30. van Gunsteren, W. F. and Berendsen, H. J. C. *J. Comp.-Aid. Mol. Des*. **1987**, *1*, 171.
31. Kang, Y. K.; Nemethy, G. and Scheraga, H. A. *J. Phys. Chem*. **1987**, *91*, 4105.
32. Kang, Y. K.; Nemethy, G. and Scheraga, H. A. *J. Phys. Chem*. **1987**, *91*, 4110.
33. Hentschke, R.; Edwards, P. J. B.; Boden, N. and Bushby, R. J. *Macromol. Symp*. **1994**, *81*, 361.
34. Lee, S. *J. Chem. Phys*. **1987**, *87*, 4972.
35. Onsager, L. *Ann. N. Y. Acad. Sci*. **1949**, *51*, 627.